International Journal of Science and Research (IJSR)
ISSN: 2319-7064
Impact Factor 2024: 7.101

Palladium-Doped Reduced Graphene Oxide Hybrid Structures for the Micro-Trace Detection of Arsenic (III) Ions

Arti[1], Naushad Alam[2], Jamilur R. Ansari[3]

[1]Department of Physics, Lalit Narayan Mithila University, Darbhanga-846004, Bihar, India
Email*: kumariarti0079[at]gmail.com*

[2]Professor, Department of Physics, Lalit Narayan Mithila University, Darbhanga-846004, Bihar, India
Corresponding Author Email: *nalam8841[at]gmail.com*

[3]Department of Applied Science, Laxmi Devi Institute of Engineering & Technology, Chikani, Alwar-301028, Rajasthan, India
Corresponding Author Email: *drjransari1[at]gmail.com*

Abstract: ***This study focuses on the synthesis techniques and characterization of graphene and reduced graphene oxide (rGO) incorporated with palladium (Pd) nanocomposites, which are essential for enhancing electrochemical sensing applications among others. The nanocomposites in question consist of palladium nanoparticles (Pd NPs) and rGO, which can be synthesized through various methods. In our synthesis approach, K_2PdCl_4 is thermally reduced at 60°C over an 80-minute duration, utilizing ascorbic acid as a reducing agent. This method facilitates the formation of Pd nanoparticles, leveraging the intrinsic properties of rGO, which possesses a substantial surface area that makes it an effective catalyst support. The extensive surface area of rGO allows for a greater density of active sites, which, when combined with Pd NPs, significantly enhances catalytic activity, particularly in processes such as ethanol oxidation, thereby improving electrochemical performance. Various characterization techniques are employed in this research, including UV-Vis, Raman, PL, TEM, and X-ray photoelectron spectroscopy (XPS). The findings provide insights into the diverse synthesis mechanisms of these nanomaterials and their effective applications in electrochemical sensing. Additionally, the investigation addresses the sustainability and reusability of the nanoparticles for long-term applications in this field.***

Keywords: Nanocomposites, electrochemical sensing, characterization, reduced graphene oxide, palladium, catalysts

1. Introduction

We are utilizing a two-dimensional nanosheet material known as graphene oxide (GO), which exhibits distinct characteristics such as an exceptional surface area, high electrical conductivity, robust thermal stability, and elevated carrier mobility[1]. The presence of numerous oxygen-containing functional groups on GO serves as nucleation centers, creating a wealth of active sites for the deposition of nanoparticles (NPs). These properties render GO an outstanding alternative to traditional carbon materials, enabling a diverse array of applications across electrochemistry, organic chemistry, and nanotechnology [2]. The versatility of GO is further enhanced through reduction processes, including light, thermal, and chemical methods[3], to yield reduced graphene oxide (rGO). In our studies, palladium (Pd) functions as an electrocatalyst, capable of facilitating various electrocatalytic reactions. It shows promising higher energy conversion efficiency while maintaining low toxicity [4]. Recently, Pd has emerged as a substitute for platinum (Pt) due to its enhanced activity and stability, alongside a favorable fit for interactions in relation to the intermediate spacing between carbon structures [5].

In alkaline environments, Pd electrocatalysts demonstrate the ability to cleave carbon-carbon (C-C) bonds in ethanol [6], an advantageous reaction for fuel cell applications [7]. A significant advantage of using Pd as an electrocatalyst [8] lies in its relative abundance in the Earth's crust and its cost-effectiveness, broadening its potential for deployment in fuel cells. In alkaline conditions, Pd NPs [9] substantially accelerate reaction rates while enhancing electroactivity. The increased surface area and the unique atomic arrangement at the edges and corners of Pd NPs amplify their catalytic activity. Notably, Pd NPs [10] can adsorb greater amounts of hydrogen compared to bulk Pd materials, underscoring their superior electrochemical performance. Despite the compelling advantages of Pd-based electrocatalysts, there are constraints that need consideration when employing them in direct ethanol fuel cells (DEFCs). Specifically, the aggregation of Pd NPs can lead to decreased catalytic activity due to elevated surface energy [11], presenting an area ripe for further investigation and optimization.

Numerous strategies have emerged to mitigate the aggregation of palladium nanoparticles (Pd NPs). These include the development of alloy catalysts utilizing single metals [12], synthesizing hybrids with relevant materials [13], and modifying the morphology of the nanoparticles [14] themselves. Notably, nickel foam (NF) has garnered attention as a proficient electrocatalyst owing to its advantageous properties such as a larger surface area [15] and open-pore structure [16], which also render it a suitable substrate for platinum (Pt) electrocatalysts. A significant technique in this realm is localized surface plasmon resonance (LSPR), which is employed to investigate the nanostructures of noble metals and their photochemical behaviors [17]. In contemporary applications, electrochemical reactions [18] are coupled with LSPR excitation of metallic nanoparticles. The LSPR excitation for Pd NPs spans the ultraviolet-visible spectrum [19], with absorbance peaks typically observed between 350 and 400 nm [20]. One specific study identified an absorbance

peak at 362 nm under LSPR excitation for Pd NPs. Additionally, polydopamine (PDA) has been recognized as an effective adhesive polymeric material thanks to its excellent conductivity and biocompatibility. PDA can be synthesized through self-polymerization from an aqueous dopamine solution in an alkaline environment, typically at pH 8.5 [21]. The incorporation of functional groups, such as amine (NH_2) groups in PDA, enhances conductivity and can effectively reduce graphene accumulation [22].

2. Materials

Palladium chloride ($Pdcl_2$), ethanol, deionized water, PVDF membrane, Sodium borohydride ($NaBH_4$), Hydrogen peroxide (H_2O_2), Polyvinylpyrrolidone (PVP), Sulphuric acid (H_2SO_4), Hydrogen chloride (HCl), Phosphoric acid (H_3PO_4), and Potassium permanganate ($KMnO_4$),

2.1 Preparation of Reduced Graphene Oxide (rGO)

Reduced graphene oxide (rGO) was synthesized via a thermal reduction of graphene oxide (GO), which was prepared through a modified Hummers' method [23]. A solution was prepared in a 250 mL flask containing a volume ratio of 9:1 of 98% H_2SO_4 to H_3PO_4, along with 0.75 g of graphite powder and 4.85 g of $KMnO_4$. This mixture was cooled in an ice-water bath before being heated to 50°C and stirred for 12 hours. Following this, the mixture was allowed to cool to room temperature, then poured onto ice. A 0.75 mL aliquot of 30% H_2O_2 was added to quench the reaction. The resulting GO was collected via centrifugation, followed by washing with 30% HCl and subsequently with 5% HCl solution. Finally, the rGO was isolated by filtration through a PVDF membrane, yielding a neutral suspension, which was then dried at ambient temperature prior to use.

2.2 Preparation of Palladium Nanoparticles (Pd NPs)

Palladium nanoparticles (Pd NPs) were prepared using a chemical reduction method. Palladium (II) chloride ($PdCl_2$) was dissolved in deionized water, and polyvinylpyrrolidone (PVP) served as a stabilizing agent to minimize nanoparticle aggregation. A reducing agent—sodium borohydride ($NaBH_4$)—was added dropwise to the $PdCl_2$ solution while stirring continuously. The transformation of the solution from a bright yellow to deep, rich dark brown, bordering on black, vividly signaled the emergence of palladium nanoparticles[24]. The reaction was maintained for an additional 30 to 60 minutes to ensure complete reduction. The resultant Pd NPs were collected by centrifugation at 8000-10000 rpm and washed multiple times with ethanol and deionized water to remove impurities. The purified Pd NPs were then dried at 60°C in a vacuum oven[25].

2.3 Preparation of Palladium-Reduced Graphene Oxide Nanocomposites (Pd-rGO)

The Pd-rGO nanocomposites were synthesized through a hydrothermal method. A mixture was created using 100 mg of GO in 50 mL of deionized water, resulting in a yellowish-black suspension. Subsequently, 1 mL of $PdCl_2$ and a stoichiometric amount of sodium hydroxide (NaOH) were added. Ethylene glycol was added dropwise, serving as a reducing agent. The reaction mixture was continuously stirred at room temperature for 6 hours. Following the reaction, the product was isolated by centrifugation at 8000 rpm for 10 minutes, cleaned extensively with deionized water, and then dried at 60°C in a vacuum oven for 24 hours.

2.4 Electrode Preparation

Electrochemical measurements were carried out on glassy carbon rotating disk electrodes (GC-RDE) that were polished using alumina slurries (0.3 µm and 0.5 µm) before cleaning with ethanol and deionized water via sonication. For catalyst ink preparation, a stable suspension was made by mixing deionized water, isopropanol, and Nafion in a volume ratio of 4:1:0.05. In the case of Pd/C catalysts, the dispersion was sonicated for 30 minutes before a 10 µL deposition on the GC-RDE (0.2471 cm^2) was performed. For the rGO-Pd composites, a 1 mg/mL dilution of the sample was prepared and sonicated for 30 minutes before applying a 10 µL drop. All experiments were conducted under identical conditions, and electrodes were dried for one hour in a fume hood prior to testing.

3. Results and Discussion

3.1 UV- Vis analysis of rGO- Pd hybrid structure

The UV-Vis absorption spectrum of the rGO-Pd hybrid structure is presented in **Figure 1**, illustrating both the intrinsic optical properties of reduced graphene oxide (rGO) and the modifications induced by the incorporation of palladium (Pd) nanoparticles. This spectrum provides critical insights into the interaction strength between rGO and Pd, as well as the alterations in electronic transitions[26]. In the wavelength range of 200-250 nm, a broad absorption feature is noted, indicative of the accumulation of Pd NPs and their plasmonic effects.

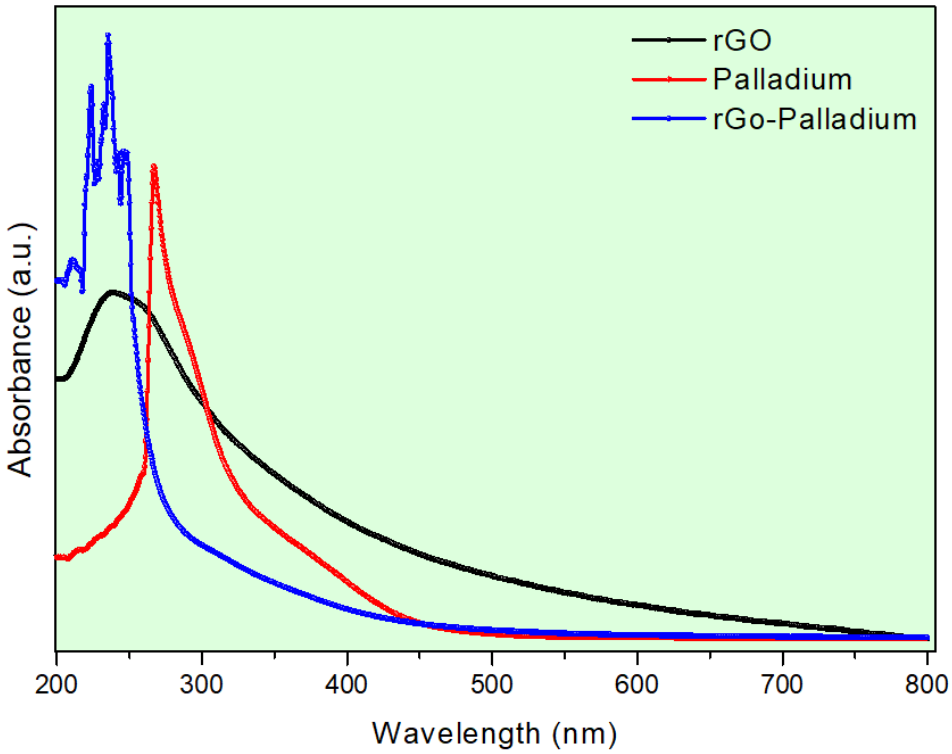

Figure 1: UV-Vis spectra of rGO-Pd hybrid structure

The free electrons within the Pd nanoparticles oscillate in this range, leading to light absorption and exhibiting interband transitions of Pd. Consequently, the Pd NPs absorb light, thereby elevating the overall absorbance of the hybrid structure. A distinct sharp peak at 270 nm corresponds to the surface plasmon resonance (SPR) of the Pd NPs and reflects the charge transfer between rGO and Pd. This peak signifies robust optical coupling between Pd and rGO, facilitating successful electronic interactions at the hybrid level. Beyond 300 nm, there is a gradual decrease in absorption, likely indicative of the excitonic transition characteristics of rGO. The incorporation of Pd significantly enhances the optical absorption in the UV-Vis range, which is pertinent for applications in photocatalysis, optoelectronics[27], and sensing, where effective light absorption is essential. Thus, the UV-Vis spectra validate the successful formation of the hybrid structure.

3.2 Photoluminescence analysis of rGO-Pd hybrid structure

The photoluminescence (PL) spectrum for the rGO-Pd hybrid structure, depicted in **Figure 2,** elucidates the electronic structure, excitonic recombination, and charge transfer dynamics within the hybrid system. As a bandgap semiconductor, rGO predominantly exhibits enhanced PL emission. However, the introduction of Pd nanoparticles leads to notable modifications in the PL spectrum due to charge transfer interactions, defect state formation, and excitation quenching—where the excitation peaks of rGO are significantly attenuated by the presence of Pd.

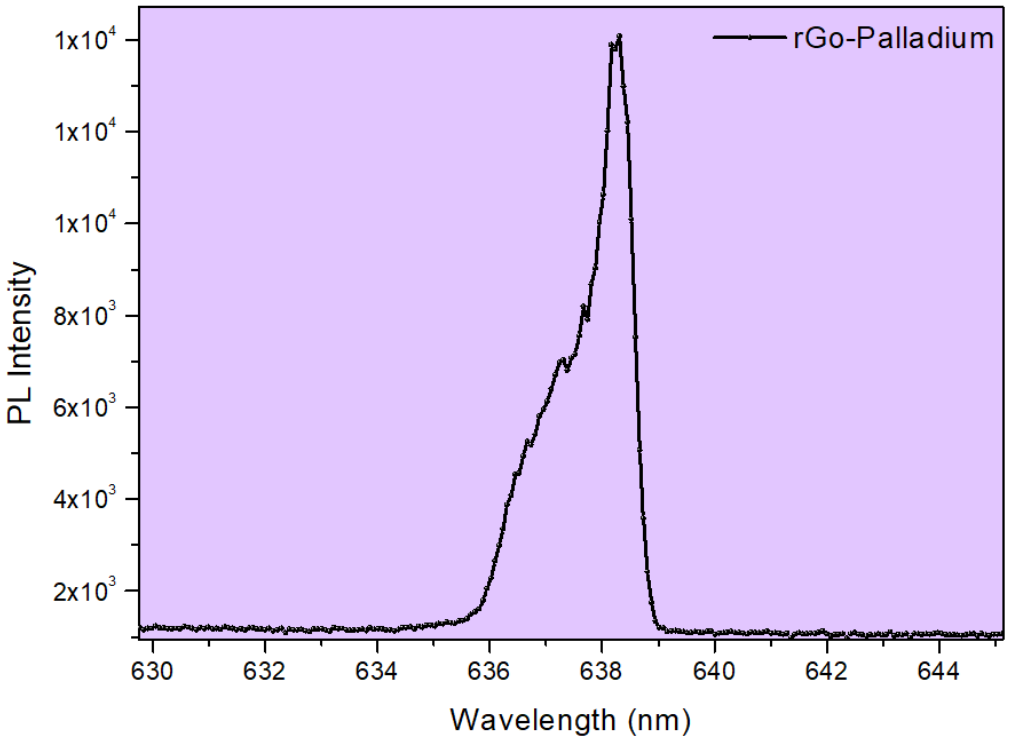

Figure 2: PL spectra of rGO-Pd hybrid structure

This quenching phenomenon arises from the additional non-radiative recombination pathways facilitated by Pd, thereby decreasing the overall PL intensity. The extent of this quenching is governed by the interaction strength between Pd and rGO, as well as the size and distribution of the nanoparticles. The PL spectrum reveals two prominent emission peaks: a sharp peak at 638 nm and a slightly lower intensity peak at 637 nm, indicating strong radiative recombination within the hybrid structure. These peaks suggest that the inclusion of Pd enhances the optical characteristics of rGO, attributed to charge transfer processes and localized surface plasmon resonance (LSPR) of the Pd nanoparticles[28]. The prominent peak at 638 nm is indicative of excitonic transitions resulting from a modified band structure due to the interaction with Pd. Moreover, this peak may also signify a secondary electronic transition, possibly stemming from defect states or localized energy levels associated with the Pd. The remaining spectral region does not exhibit additional peaks, reinforcing the dominance of the 637-638 nm peaks in the PL response.

3.3 Raman analysis of rGO-Pd hybrid structure

The Raman spectra of the rGO-Pd hybrid structure, illustrated in **Figure 3**, provides critical insights into its vibrational modes, structural characteristics, and the interplay between palladium (Pd) nanoparticles and reduced graphene oxide (rGO). The intensity plotted against Raman shift reveals well-defined peaks that correspond to the phonon modes of rGO, along with additional features attributed to the incorporation of Pd nanoparticles. Notably, the spectrum reflects various modifications that illuminate strain effects, vibrational modes, and electron-phonon interactions. Through Raman spectroscopy[29], we can characterize structural aspects such as double carbon-carbon bonds and electron-phonon coupling in graphene[30]. The prominent peak, referred to as the G peak, appears at approximately 1600 cm^{-1}, resulting from first-order scattering of sp^2 carbon atoms in the E_{2g} mode[31]. A secondary peak, identified as the D peak, manifests at 1350 cm^{-1}, indicative of structural defects or grain boundaries typical of amorphous carbon. The spectra indicate that the reduction of graphene oxide (GO) to rGO was successfully achieved following annealing. It is evident in the figure that the G peak of the GO-Pd hybrid corresponds to 1600 cm^{-1} and the D peak of the rGO-Pd composite aligns at 1351 cm^{-1}. The intensity ratio (I_D/I_G) between the D and G peaks serves as a measure of defect density and the extent of graphitization in the graphene material[32]. For the GO-Pd nanocomposite, the I_D/I_G ratio is 0.93, exceeding the rGO-Pd ratio of 0.89, which indicates a higher defect density in the GO structure compared to rGO, thereby confirming the reduction process post-annealing.

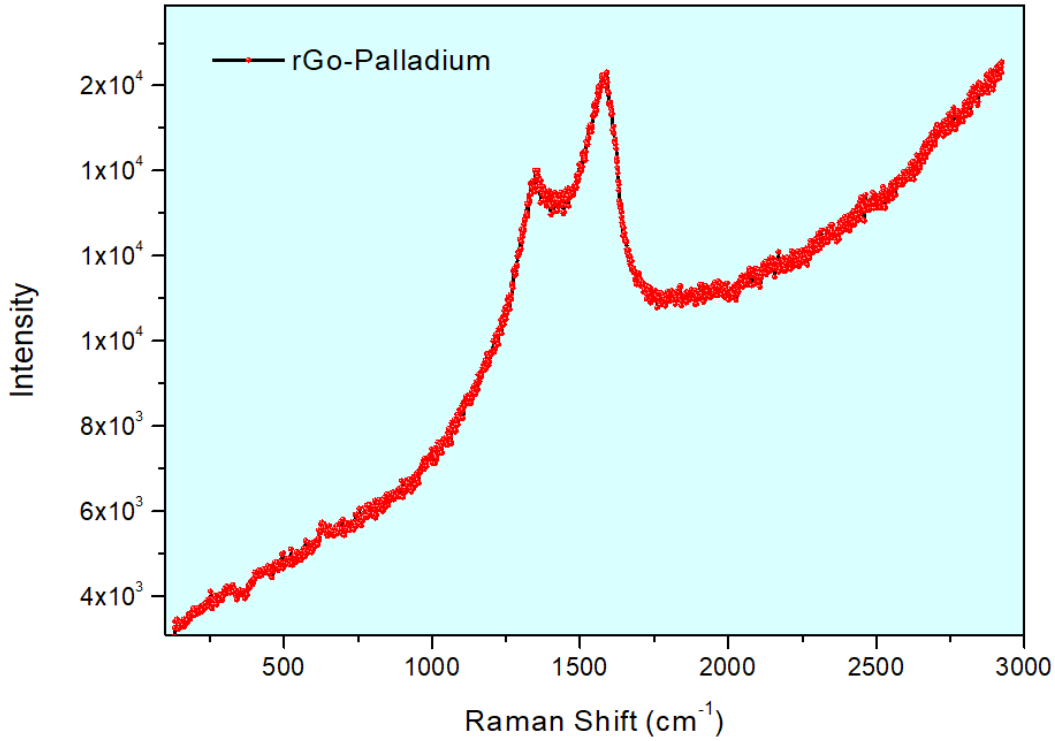

Figure 3: Raman spectra of rGO-Pd hybrid structure

3.4 TEM analysis of rGO-Pd hybrid structure

The morphology and structural features of the rGO-Pd hybrid material were performed by TEM. The TEM and HRTEM images reveal a uniform distribution of Pd nanoparticles on the graphene surface **(Figure 4a)**. The observed wrinkling of the graphene sheets signifies the inherent flexibility of rGO, while the uniformity in Pd distribution suggests a strong interaction between the Pd and rGO. Certain regions exhibit noticeable agglomeration of Pd nanoparticles. In **Figure 4(b),** a scale of 20 nm is employed to closely view the Pd distribution on rGO; most nanoparticles adhere to a specific size range, although some variability in diameter is presented in the histogram. A narrow distribution depicted in the histogram indicates a well-controlled synthesis process, whereas a broader distribution reflects size variation in the hybrid structure. The uniform dispersion of Pd nanoparticles signifies effective hybridization; the observed size variation implies constraints in growth during the synthesis. The darker regions in the imagery represent Pd-rich zones, suggesting localized aggregation. **Figure 4(c)** applies a high magnification at a 2 nm scale, confirming the crystalline nature of the hybrid, characterized by clear lattice fringes. An interplanar spacing of 0.225 nm correlates with the (111) planes of Pd within the rGO-Pd composites, supporting the structural integrity of the material. The lattice fringes indicate a crystalline Pd with minimal defects, indicative of a robust interaction between the components of the hybrid. Bright spots identified as Pd on rGO signify incorporation without inducing lattice distortion. Lastly, **Figure 4(d)** presents a broader view of the hybrid's morphology, wherein the rGO exhibits a sheet-like structure with dark spots representing incorporated Pd nanoparticles, an essential feature for sustaining the electronic and catalytic properties of the composite.

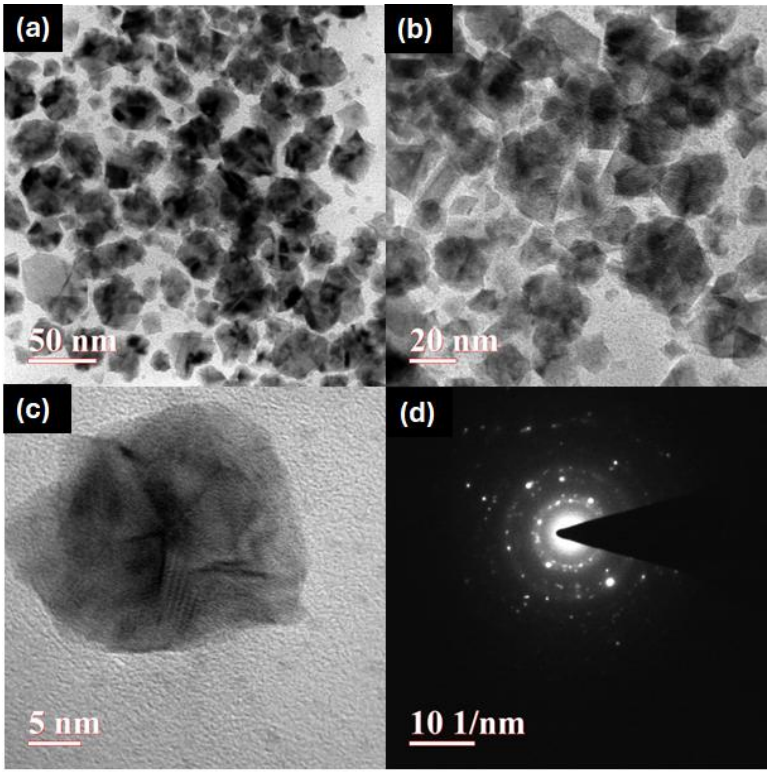

Figure 4: TEM analysis of (a,b) rGO-Pd hybrid structure (c) HRTEM of Pd NPs and (d) SAED of rGO-Pd hybrid structures

3.5 XPS analysis of rGO-Pd hybrid structure

X-Ray Photoelectron Spectroscopy (XPS) provides valuable insights into the composition and structural characteristics of composite materials, thereby augmenting our understanding of their properties. The XPS spectra effectively characterize the components within the hybrid, elucidating the chemical states of the constituents and shedding light on the surface characteristics of the particles. In **Figure 5a**, the complete XPS spectrum for reduced graphene oxide (rGO), palladium (Pd), and the rGO-Pd composite is presented, revealing the presence of carbon, nitrogen, oxygen, and palladium species. For the three composites examined, a peak at 284 eV corresponds to the C 1s feature, while the peak at 530 eV indicates the O 1s transition **(Figure 5d)**. The N 1s feature is identified at 400 eV. Furthermore, a Pd 3d peak is observed at 338 eV, indicating that the Pd nanoparticles were deposited uniformly onto the surface of the graphene oxide **(Figure 5b)**.

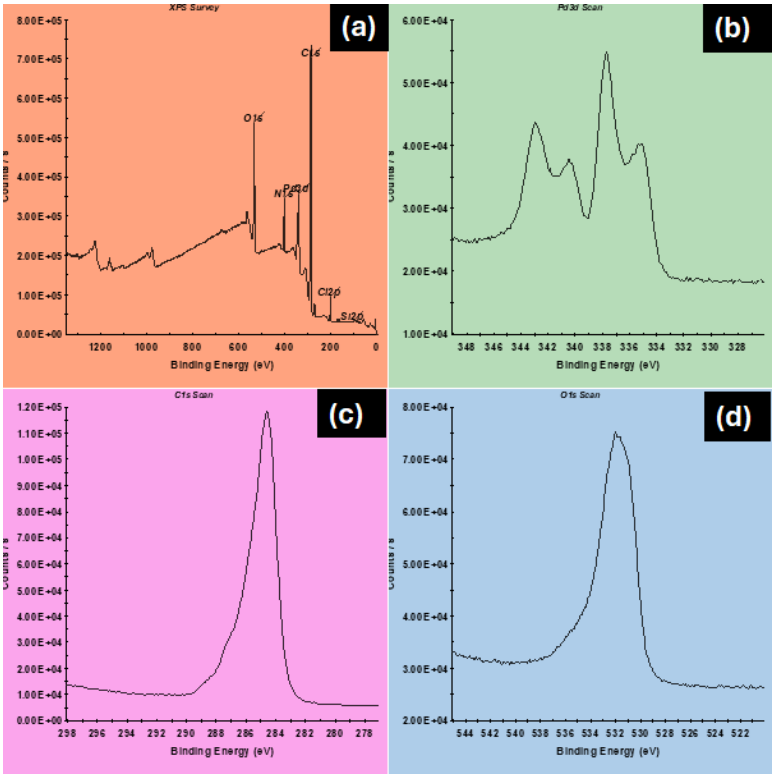

Figure 5: XPS analysis of rGO-Pd hybrid structure (a) Survey (b)Pd 3d (c) C1s and (d) O1s

The C 1s spectrum for Pd/GO displays a peak with binding energies at 284.5 eV, which is attributed to C-C, bonding. In comparison, the C 1s spectrum of Pd/rGO presents a peak at binding energies of 284.5 eV, correlating with the contributions of C-C bond [33] **(Figure 5c)**. The annealing process induces differences between Pd/GO and Pd/rGO, where internal stresses are alleviated, reducing hardness and enhancing interaction between the Pd and GO. The Pd 3d peaks in the XPS spectrum for Pd/GO comprise two features: a binding energy of 335.0 eV for Pd 3d5/2 and 340.1 eV for Pd 3d3/2, indicating the presence of Pd(0)[34]. Additionally, a weaker pair at 336.9 eV and 342.4 eV for Pd 3d5/2 and Pd 3d3/2, respectively, suggests the presence of Pd(II)[35]. The binding energy associated with Pd/rGO in the Pd 3d state is elevated compared to the Pd/GO composite, indicating a modification in the electronic structure and a potential shift in the Fermi level[36] of the d-band.

3.6 Sensor performance of Arsenic analysis using DPV

In terms of sensor performance for arsenic analysis using Differential Pulse Voltammetry (DPV), the electrochemical sensing capabilities of the rGO-Pd hybrid were evaluated. The DPV measurements were systematically recorded while varying the concentration of As(III) from 0.1 to 1.0 parts per billion (ppb), at a scan rate of 10 mV/s and within a potential range of 0.1 to 0.4 V **(Figure 6)**. The DPV curve analysis indicates a distinct variation in shape and magnitude as the concentration of arsenic in the solution [37] varies. Notably, as arsenic levels increase[38], we observe a shift in potential alongside an enhancement of the oxidation peak current, signaling improved electrocatalytic properties of the rGO-Pd hybrid structure employed for arsenic detection in biological systems. The investigation was conducted at a pH of 6.0, which resulted in a reduced oxidation peak.

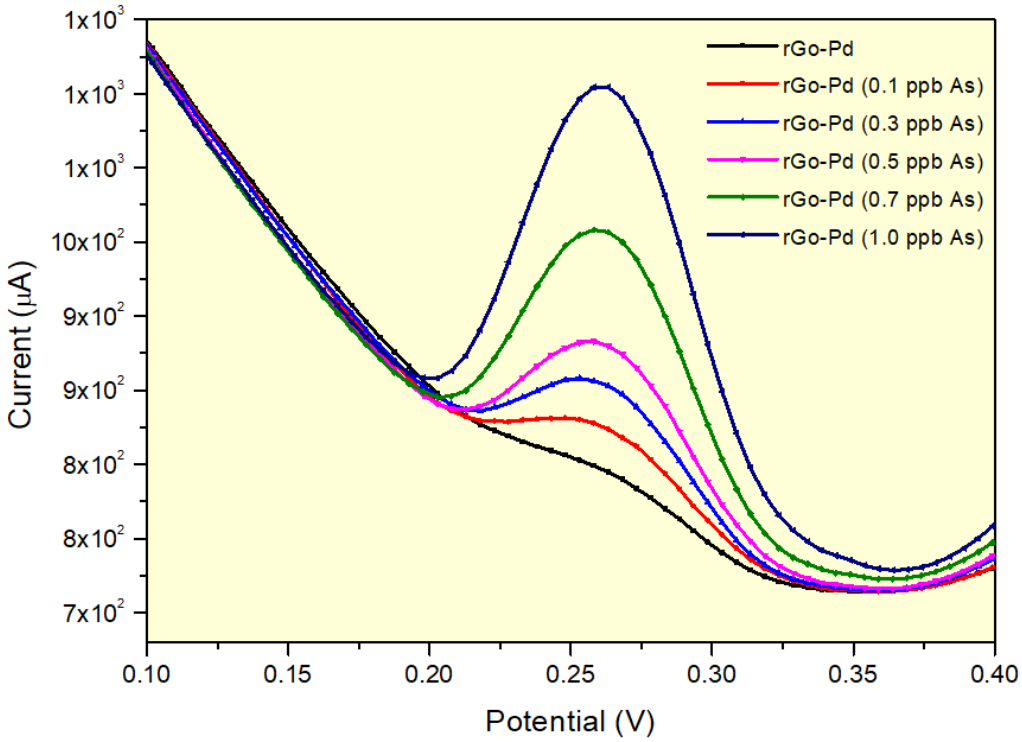

Figure 6: Differential Pulse Voltammetry (DPV) response of rGO-Pd hybrid structure with Arsenic concentrations varying from 0.1-1.0 ppb.

A redox reaction is occurring at the electrode, reflecting a transition between the cathodic and anodic peaks, indicative of pseudocapacitive behavior. The reversible interaction between Pd ions and the solution interface contributes to this behavior, underscoring the electrochemical sensing performance of the rGO-Pd composite. The peak potential recorded is 0.26 V, and an increase in As(III) concentration from 0.1 ppb to 1.0 ppb correlates with a rise in the anodic peak current. This increment suggests a larger accessible surface area on the electrode, thereby enhancing its electrocatalytic characteristics. The integration of Pd nanoparticles with reduced graphene oxide (rGO) significantly augments the electrocatalytic oxidation process. Comparatively, the rGO-Pd hybrid demonstrates a larger differential pulse voltammetry (DPV) response area than pristine Pd nanoparticles, leading to increased charge storage[39] capacity as reflected in a higher DPV response peak. Thus, it can be deduced that the incorporation of rGO enhances the capacitance of the Pd nanoparticles.

$$Cs = I\,\Delta t / m\,\Delta E$$

where
Cs – Specific capacitance
I – Discharge current
Δt–Discharge time
m – Active mass of the electrodes
ΔE – IR discharge drops

Data analysis indicates that increased current density is associated with decreased specific capacitance of the electrodes—characteristics of pseudocapacitance that improve electrochemical sensing applications. Notably, this decrease in specific capacitance translates to an increase in current, which ultimately reduces ion discharge time across

the electrodes. The results illustrate that as current density rises, discharge time diminishes, leading to a voltage drop across the electrodes, which reflects a modification in the specific capacitance attributable to the rGO-Pd hybrid structure [40]. This enhancement in overall performance, characterized by increased specific capacitance, results in a greater number of nucleation sites for energy storage. Additionally, the embedding of palladium nanoparticles onto the reduced graphene oxide matrix boosts electron transport both at the surface and within the rGO-Pd hybrid framework, significantly improving the electrode's performance and efficiency, alongside a reduction in resistance that broadens its practical applications.

4. Conclusion

We have successfully synthesized Pd nanoparticles (NPs), reduced graphene oxide (rGO), and rGO-Pd nanocomposites, with characterization revealing significant enhancement in the physiochemical properties of rGO due to the integration of active Pd NPs. Characterization techniques suggest that the formation of the rGO-Pd hybrid structure increases surface area while improving stability and conductivity. The interaction between rGO and Pd NPs enhances charge transfer dynamics and catalytic efficiency, positioning this material as advantageous for applications in energy storage devices, biosensors, and fuel cells. UV-Vis spectroscopy provides insights into the structural and optical properties of the rGO-Pd hybrid, promoting its utility in optoelectronic and catalytic applications. Additionally, Raman analysis and TEM/HRTEM studies further validate its versatility across various fields. The sensor performance for arsenic detection via DPV highlights the applicability of the rGO-Pd hybrid in catalysis, sensing, and energy storage technologies.

Credit authorship contribution agreement

Arti: Methodology, Investigation, Visualization, Writing – original draft, Writing – review & editing. **Naushad Alam** and **Jamilur R. Ansari:** Supervision, Validation, Project administration, funding acquisition. All the authors have read and discussed the data and agreed to the published version of the manuscript.

Acknowledgements

Arti and **Naushad Alam** gratefully acknowledge the support from LNMU in the form of a Research Fellowship. The authors thank Yonsei University for carrying out TEM/HRTEM characterizations. **Jamilur R. Ansari** is thankful to Yonsei University, South Korea, for the support under the BP Program.

References

[1] C. Wang, D. Astruc, Recent developments of metallic nanoparticle-graphene nanocatalysts, Progress in Materials Science 94 (2018) 306–383. https://doi.org/10.1016/j.pmatsci.2018.01.003.

[2] G. Manasa, R.J. Mascarenhas, S.J. Malode, N.P. Shetti, Graphene-based electrochemical immunosensors for early detection of oncomarker carcinoembryonic antigen, Biosensors and Bioelectronics: X 11 (2022) 100189. https://doi.org/10.1016/j.biosx.2022.100189.

[3] L. Zhang, T. Wu, X. Xu, F. Xia, H. Na, Y. Liu, H. Qiu, W. Wang, J. Gao, Magnetic bimetallic nanoparticles supported reduced graphene oxide nanocomposite: Fabrication, characterization and catalytic capability, Journal of Alloys and Compounds 628 (2015) 364–371. https://doi.org/10.1016/j.jallcom.2014.11.207.

[4] Y. Tao, A. Dandapat, L. Chen, Y. Huang, Y. Sasson, Z. Lin, J. Zhang, L. Guo, T. Chen, Pd-on-Au Supra-nanostructures Decorated Graphene Oxide: An Advanced Electrocatalyst for Fuel Cell Application, Langmuir 32 (2016) 8557–8564. https://doi.org/10.1021/acs.langmuir.6b01382.

[5] A. A. El-Shafei, A.M. Abd Elhafeez, H.A. Mostafa, Ethanol oxidation at metal–zeolite-modified electrodes in alkaline medium. Part 2: palladium–zeolite-modified graphite electrode, J Solid State Electrochem 14 (2010) 185–190. https://doi.org/10.1007/s10008-009-0872-8.

[6] Z. Zhang, L. Xin, K. Sun, W. Li, Pd–Ni electrocatalysts for efficient ethanol oxidation reaction in alkaline electrolyte, International Journal of Hydrogen Energy 36 (2011) 12686–12697. https://doi.org/10.1016/j.ijhydene.2011.06.141.

[7] C.W. Xu, H. Wang, P.K. Shen, S.P. Jiang, Highly Ordered Pd Nanowire Arrays as Effective Electrocatalysts for Ethanol Oxidation in Direct Alcohol Fuel Cells, Advanced Materials 19 (2007) 4256–4259. https://doi.org/10.1002/adma.200602911.

[8] A.K. Ipadeola, R. Barik, S.C. Ray, K.I. Ozoemena, Bimetallic Pd/SnO2 Nanoparticles on Metal Organic Framework (MOF)-Derived Carbon as Electrocatalysts for Ethanol Oxidation, Electrocatalysis 10 (2019) 366–380. https://doi.org/10.1007/s12678-019-00518-5.

[9] A. Zalineeva, S. Baranton, C. Coutanceau, G. Jerkiewicz, Electrochemical Behavior of Unsupported Shaped Palladium Nanoparticles, Langmuir 31 (2015) 1605–1609. https://doi.org/10.1021/la5025229.

[10] A. Zalineeva, S. Baranton, C. Coutanceau, G. Jerkiewicz, Octahedral palladium nanoparticles as excellent hosts for electrochemically adsorbed and absorbed hydrogen, Sci. Adv. 3 (2017) e1600542. https://doi.org/10.1126/sciadv.1600542.

[11] M. Gopiraman, D. Deng, K.-Q. Zhang, W. Kai, I.-M. Chung, R. Karvembu, I.S. Kim, Utilization of Human Hair as a Synergistic Support for Ag, Au, Cu, Ni, and Ru Nanoparticles: Application in Catalysis, Ind. Eng. Chem. Res. 56 (2017) 1926–1939. https://doi.org/10.1021/acs.iecr.6b04209.

[12] C.-C. Kung, P.-Y. Lin, Y. Xue, R. Akolkar, L. Dai, X. Yu, C.-C. Liu, Three dimensional graphene foam supported platinum–ruthenium bimetallic nanocatalysts for direct methanol and direct ethanol fuel cell applications, Journal of Power Sources 256 (2014) 329–335. https://doi.org/10.1016/j.jpowsour.2014.01.074.

[13] Q. Zhang, L. Jiang, H. Wang, J. Liu, J. Zhang, Y. Zheng, F. Li, C. Yao, S. Hou, Hollow Graphitized Carbon Nanocage Supported Pd Catalyst with Excellent Electrocatalytic Activity for Ethanol Oxidation, ACS Sustainable Chem. Eng. 6 (2018) 7507–7514. https://doi.org/10.1021/acssuschemeng.8b00208.

[14] M. Li, P. Liu, R.R. Adzic, Platinum Monolayer Electrocatalysts for Anodic Oxidation of Alcohols, J. Phys. Chem. Lett. 3 (2012) 3480–3485. https://doi.org/10.1021/jz3016155.

[15] J. Van Drunen, B. Kinkead, M.C.P. Wang, E. Sourty, B.D. Gates, G. Jerkiewicz, Comprehensive Structural, Surface-Chemical and Electrochemical Characterization of Nickel-Based Metallic Foams, ACS Appl. Mater. Interfaces 5 (2013) 6712–6722. https://doi.org/10.1021/am401606n.
[16] M. Grdeń, M. Alsabet, G. Jerkiewicz, Surface Science and Electrochemical Analysis of Nickel Foams, ACS Appl. Mater. Interfaces 4 (2012) 3012–3021. https://doi.org/10.1021/am300380m.
[17] S. Marhaba, N. El Kawni, LOCALIZED SURFACE PLASMON RESONANCE OF PALLADIUM PARALLELEPIPED NANOPARTICLES, BAU Journal - Science and Technology 4 (2023). https://doi.org/10.54729/2959-331X.1093.
[18] B.S. Hoener, S.R. Kirchner, T.S. Heiderscheit, S.S.E. Collins, W.-S. Chang, S. Link, C.F. Landes, Plasmonic Sensing and Control of Single-Nanoparticle Electrochemistry, Chem 4 (2018) 1560–1585. https://doi.org/10.1016/j.chempr.2018.04.009.
[19] C. Xu, F. Qin, Q. Zhu, J. Lu, Y. Wang, J. Li, Y. Lin, Q. Cui, Z. Shi, A.G. Manohari, Plasmon-enhanced ZnO whispering-gallery mode lasing, Nano Res. 11 (2018) 3050–3064. https://doi.org/10.1007/s12274-018-2047-3.
[20] A. Kalaiselvi, S.M. Roopan, G. Madhumitha, C. Ramalingam, G. Elango, Synthesis and characterization of palladium nanoparticles using Catharanthus roseus leaf extract and its application in the photo-catalytic degradation, Spectrochimica Acta Part A: Molecular and Biomolecular Spectroscopy 135 (2015) 116–119. https://doi.org/10.1016/j.saa.2014.07.010.
[21] H. Lee, S.M. Dellatore, W.M. Miller, P.B. Messersmith, Mussel-Inspired Surface Chemistry for Multifunctional Coatings, Science 318 (2007) 426–430. https://doi.org/10.1126/science.1147241.
[22] G. Liu, S. Lu, W. Xu, G. He, Y. Zheng, Y. Cheng, Fabrication of graphene/copper–nickel foam composite for high performance supercapacitors, New J. Chem. 42 (2018) 9455–9462. https://doi.org/10.1039/C8NJ01017J.
[23] D.C. Marcano, D.V. Kosynkin, J.M. Berlin, A. Sinitskii, Z. Sun, A. Slesarev, L.B. Alemany, W. Lu, J.M. Tour, Improved Synthesis of Graphene Oxide, ACS Nano 4 (2010) 4806–4814. https://doi.org/10.1021/nn1006368.
[24] A. Chen, C. Ostrom, Palladium-Based Nanomaterials: Synthesis and Electrochemical Applications, Chem. Rev. 115 (2015) 11999–12044. https://doi.org/10.1021/acs.chemrev.5b00324.
[25] M.V. Bravo, O.F. Silva, C. Adam, A.M. Granados, A simple way to prepare palladium nanoparticles decorated with cyclodextrins and ionic liquid. The effects of coating on the catalytic activity and colloidal stability, Journal of Molecular Liquids 304 (2020) 112725. https://doi.org/10.1016/j.molliq.2020.112725.
[26] R. Ribeiro-Palau, C. Zhang, K. Watanabe, T. Taniguchi, J. Hone, C.R. Dean, Twistable electronics with dynamically rotatable heterostructures, Science 361 (2018) 690–693. https://doi.org/10.1126/science.aat6981.
[27] P.V. Pham, S.C. Bodepudi, K. Shehzad, Y. Liu, Y. Xu, B. Yu, X. Duan, 2D Heterostructures for Ubiquitous Electronics and Optoelectronics: Principles, Opportunities, and Challenges, Chem. Rev. 122 (2022) 6514–6613. https://doi.org/10.1021/acs.chemrev.1c00735.
[28] K.M. Mayer, J.H. Hafner, Localized Surface Plasmon Resonance Sensors, Chem. Rev. 111 (2011) 3828–3857. https://doi.org/10.1021/cr100313v.
[29] S. Sahoo, G. Khurana, S.K. Barik, S. Dussan, D. Barrionuevo, R.S. Katiyar, In Situ Raman Studies of Electrically Reduced Graphene Oxide and Its Field-Emission Properties, J. Phys. Chem. C 117 (2013) 5485–5491. https://doi.org/10.1021/jp400573w.
[30] K.N. Kudin, B. Ozbas, H.C. Schniepp, R.K. Prud'homme, I.A. Aksay, R. Car, Raman Spectra of Graphite Oxide and Functionalized Graphene Sheets, Nano Lett. 8 (2008) 36–41. https://doi.org/10.1021/nl071822y.
[31] B. He, Z. Ren, S. Yan, Z. Wang, Large area uniformly oriented multilayer graphene with high transparency and conducting properties derived from highly oriented polyethylene films, J. Mater. Chem. C 2 (2014) 6048–6055. https://doi.org/10.1039/C4TC00481G.
[32] J. Balamurugan, T.D. Thanh, S.-B. Heo, N.H. Kim, J.H. Lee, Novel route to synthesis of N-doped graphene/Cu–Ni oxide composite for high electrochemical performance, Carbon 94 (2015) 962–970. https://doi.org/10.1016/j.carbon.2015.07.087.
[33] Y. Zheng, S. Lu, W. Xu, G. He, Y. Cheng, T. Yu, Y. Zhang, The fabrication of graphene/polydopamine/nickel foam composite material with excellent electrochemical performance as supercapacitor electrode, Journal of Solid State Chemistry 258 (2018) 401–409. https://doi.org/10.1016/j.jssc.2017.11.006.
[34] S. Fu, C. Zhu, D. Du, Y. Lin, Facile One-Step Synthesis of Three-Dimensional Pd–Ag Bimetallic Alloy Networks and Their Electrocatalytic Activity toward Ethanol Oxidation, ACS Appl. Mater. Interfaces 7 (2015) 13842–13848. https://doi.org/10.1021/acsami.5b01963.
[35] Y. Zhai, Z. Zhu, X. Lu, Z. Zhou, J. Shao, H.S. Zhou, Facile Synthesis of Three-Dimensional PtPdNi Fused Nanoarchitecture as Highly Active and Durable Electrocatalyst for Methanol Oxidation, ACS Appl. Energy Mater. 1 (2018) 32–37. https://doi.org/10.1021/acsaem.7b00032.
[36] H. Zhang, Y. Yin, Y. Hu, C. Li, P. Wu, S. Wei, C. Cai, Pd@Pt Core−Shell Nanostructures with Controllable Composition Synthesized by a Microwave Method and Their Enhanced Electrocatalytic Activity toward Oxygen Reduction and Methanol Oxidation, J. Phys. Chem. C 114 (2010) 11861–11867. https://doi.org/10.1021/jp101243k.
[37] Madhavi, M. Kumar, J.R. Ansari, V. Kumar, S. Nagar, A. Sharma, Fe3O4 Coated SiO2 Magnetic Nanoparticles for Enhanced Antibacterial Activity and Electrochemical Sensing, Metals 12 (2022) 2145. https://doi.org/10.3390/met12122145.
[38] S. Agrahari, A.K. Singh, I. Tiwari, S. Srikrishna, Electrochemical deposition of Pd on MoS2 supported graphene nanoflakes over functionalised MWCNTs as an immunosensor for detection of lung cancer biomarker, Microchemical Journal 196 (2024) 109698. https://doi.org/10.1016/j.microc.2023.109698.

[39] P. Das, Z.-S. Wu, F. Li, J. Liang, H.-M. Cheng, Two-dimensional energy materials: Opportunities and perspectives, Energy Storage Materials 22 (2019) 15–17. https://doi.org/10.1016/j.ensm.2019.03.014.
[40] L. Changshi, Reliable and precise evaluation energy-transfer and efficiency of super-capacitors, Renewable and Sustainable Energy Reviews 151 (2021) 111566. https://doi.org/10.1016/j.rser.2021.111566.